AGU PUBLICATIONS

Geophysical Research Letters

RESEARCH LETTER
10.1002/2014GL062470

Key Points:
- Fractal gradings in fault gouges are controlled by mixing and crushing
- Lognormal gradings in avalanches are controlled by crushing and segregation
- A multiscale model has been proposed for grading evolution in natural hazards

Correspondence to:
B. Marks,
benjy.marks@fys.uio.no

Citation:
Marks, B., and I. Einav (2015), A mixture of crushing and segregation: The complexity of grainsize in natural granular flows, *Geophys. Res. Lett.*, *42*, 274–281, doi:10.1002/2014GL062470.

Received 7 NOV 2014
Accepted 8 JAN 2015
Accepted article online 13 JAN 2015
Published online 25 JAN 2015

A mixture of crushing and segregation: The complexity of grainsize in natural granular flows

Benjy Marks[1,2] and Itai Einav[2,3]

[1]Condensed Matter Physics, Department of Physics, University of Oslo, Oslo, Norway, [2]Particles and Grains Laboratory, School of Civil Engineering, The University of Sydney, Sydney, Australia, [3]Department of Civil, Geomatic, and Environmental Engineering, University College London, London, UK

Abstract The interplay between grain crushing and segregation controls the dynamics of dense granular flows that underpin many natural hazards. We address this issue for the first time by developing a simple lattice model with three interacting rules—for grain crushing, mixing, and segregation. In earthquake faults, particles are trapped, they crush and mix, but do not segregate. In this case the model produces power law distributions, consistent with previous models. When segregation by kinetic sieving is added to the model, we predict depth-dependent lognormal distributions as previously observed, but not explained, in pyroclastic flows, debris flows, rock avalanches, and dry snow avalanches.

1. Introduction

When dealing with granular materials—a conglomerated system of many distinct solid particles—it is useful to classify their behavior in terms of the sizes of the grains in the system. Good examples of granular materials include sand, snow pellets, and coffee. In each case, their properties depend on their size. For example, according to *Weibull* [1951], the resistance of individual particles to crushing is statistically higher for smaller particles, while *Bagnold* [1954] showed through experiments that the shear strength of flowing granular materials increases quadratically with grain diameter for monodisperse systems—where particles are of similar size.

Natural granular materials such as sand and snow pellets are inevitably polydisperse (not monodisperse). Where they advect, for example, during geophysical flows, we need to account for variations of the grainsize distribution. We have used the term "grainsize" instead of "grain size" to highlight its possible role as an internal coordinate in continuum mechanics [*Marks et al.*, 2012]. The problem addressed here is the interaction between grainsizes as they crush, mix, and segregate. These processes are common to geophysical flows of granular materials, including earthquake fault gouges, rock avalanches, pyroclastic flows, debris flows, and snow avalanches—all of which go through indefinite shear deformation. In each case, one can ask the question: Which properties of the flow control the evolution of the grainsize distribution?

Figure 1 contains grainsize distributions collated from many studies of field data. In the case of earthquake faults, when one samples directly from the fault core, power law grainsize distributions are often recovered, independent of fault kinematics (see Figure 1a) [*Marone and Scholz*, 1989; *An and Sammis*, 1994; *Chester et al.*, 2005; *Billi*, 2005, 2007]. When such results are sorted by increasing deformation, we see a corresponding increase in the measured slope of the power law distribution (see Figure 1b, where gouge concentration is used as a proxy for deformation [*Marone and Scholz*, 1989; *Billi*, 2005]). Conversely, for snow avalanches, pyroclastic flows, debris flows, and rock avalanches, either unimodal or bimodal lognormal grainsize distributions can be observed (a lognormal distribution appears as bell-shaped on semi-logarithmic axes, see Figures 1c–1f) [*Bartelt and McArdell*, 2009; *Wilson*, 1985; *Esposito et al.*, 2013; *Phillips and Davies*, 1991; *Schmincke*, 1967; *Dunning*, 2006; *Pollet and Schneider*, 2004]. In each of these latter cases, a granular material flows down a slope, while crushing, mixing, and segregating. Even though there are large differences in the rheology of each flow, qualitatively similar grainsize distributions are produced. We propose the first mechanism to reproduce this behavior using a new lattice model with only three simple rules. Each of these rules alone will yield previously known results, but when combined, new complex phenomena emerge.

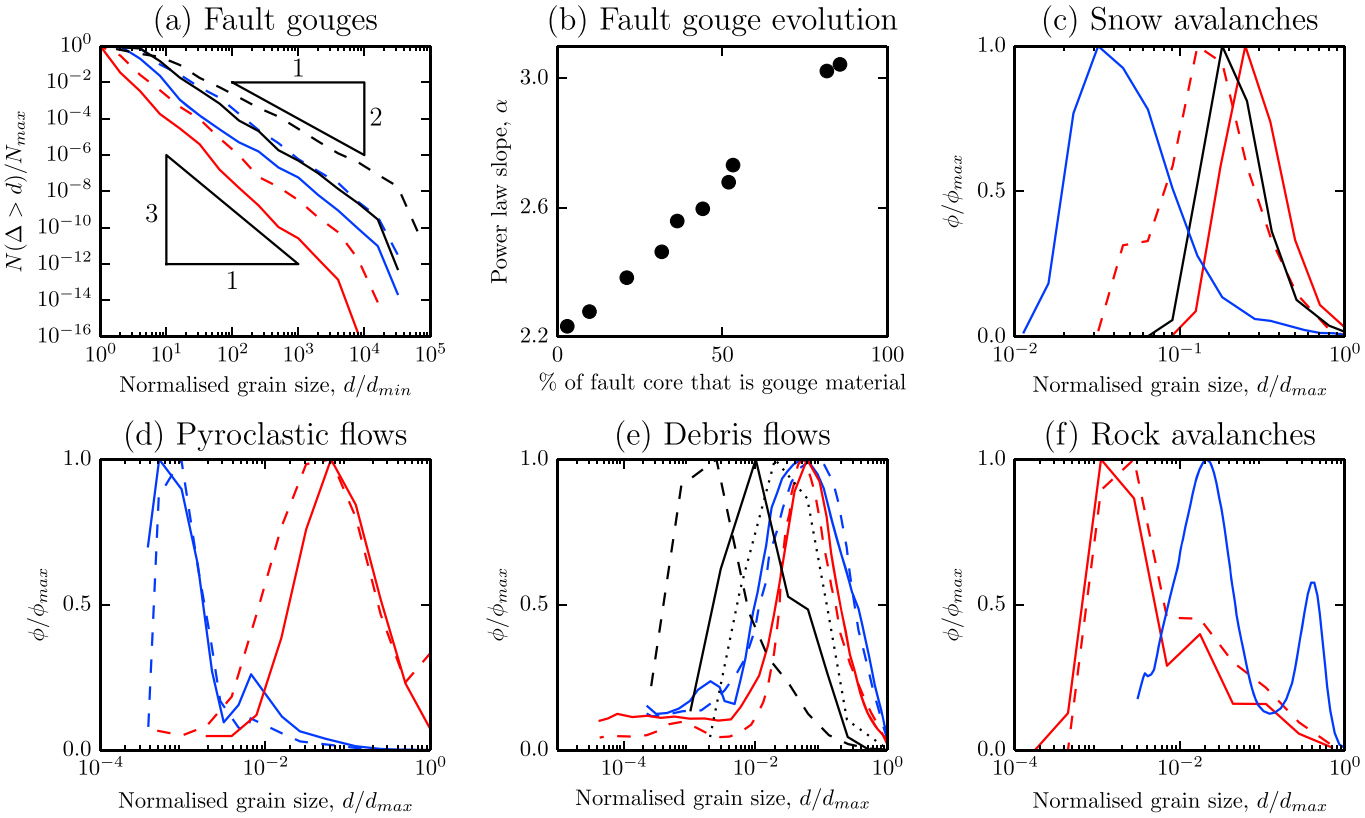

Figure 1. Typical grainsize distributions collected from published field data. (a) Grainsize distributions from six loose Mesozoic carbonate earthquake fault gouges in central Italy [*Billi*, 2007]; reverse faults (red), extensional faults (black), a strike-slip fault (solid blue) and a transpressive fault (dashed blue). (b) Fault gouge evolution from the Mattinata Fault [*Billi*, 2005]. Each point indicates a different location along the fault. The slope of the best fit power law for the gouge material is plotted against the percentage of the fault occupied by gouge material—the remaining amount being breccia. This is interpreted as a proxy for deformation. (c) Grainsize distributions from four snow avalanches [*Bartelt and McArdell*, 2009]. Two dry powder avalanches in Vallée de la Sionne (red) and two wet snow avalanches, one in Grünbödeli (black) and one in Gatschiefer (blue). (d) Grainsize distributions from pyroclastic flows. Mount Taupo, NZ, sampled 25 km from the vent [*Wilson*, 1985], at the top of each of two distinct layers composed mostly of pumice and lithics (red) and Guiliano, Italy [*Esposito et al.*, 2013], composed of Pozzolan (blue). (e) Grainsize distributions from debris flows. Samples from two flows at the Tarndale Slip, NZ, generated from clay-rich stony regoliths (red) and two from Bullock Creek, NZ, generated from highly sheared sandstone and argillite (blue) [*Phillips and Davies*, 1991], and a lahar (black) in the Ellensburg Formation, USA [*Schmincke*, 1967], sampled at top (solid), central (dashed), and basal (dotted) depths. (f) Grainsize distributions from rock avalanches. Two samples taken from an avalanche in Falling Mountain, NZ, composed of argillite and grewyacke [*Dunning*, 2006] at 3 km from the source of the avalanche (red), and one sample from the Holocene Flims sturzstrom [*Pollet and Schneider*, 2004], composed of calcareous breccia deposits (blue).

2. Results

The stochastic lattice model defined here is composed of a regular 2-D grid, portrayed in Figure 2, where each cell is located at a position $\{i, j\}$. The i index denotes a microscale internal coordinate, which not only discretizes the grainsize distribution but also preserves information on local neighbors. In the jth row, the ith cell contains an $n_{i,j}$ number of grains of identical grainsize $s_{i,j}$. All cells have the same solid fraction and volume; therefore, the number of grains scales as $n_{i,j} \propto s_{i,j}^{-3}$. The j direction represents an external coordinate, such that each row i describes the grainsize distribution of the representative volume element situated in the physical location j. In the i direction, we use many cells, such that upon averaging, this system could describe smooth grainsize distributions. Additionally, the system is periodic in the i direction and has a thickness $W = 1$ in the j direction, such that each cell has a physical thickness of ΔW.

We will now present the three rules which will facilitate crushing, mixing, and segregation. For the case of crushing, information is required at the microscale, such that the rule operates in the i direction alone. In the cases of mixing and segregation, the converse is true, and the mechanisms account for advection in physical space, such that the rules move particles in the j direction. Finally, to explore the interactions between crushing, mixing, and segregation, the rules will act simultaneously in their corresponding direction.

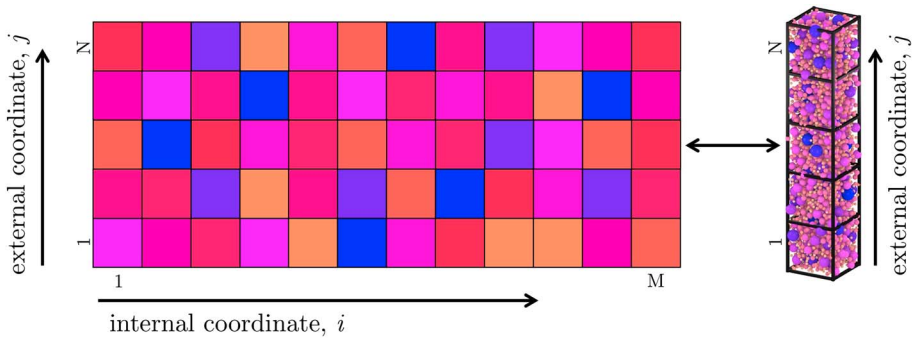

Figure 2. Schematic representation of the stochastic lattice model. On the right is the physical system we wish to represent—a polydisperse sample of granular material discretized in a single physical direction *j* into *N* representative volume elements. On the left is the equivalent stochastic lattice model, with coordinate *i* mapping the grainsize distribution discretely into *M* cells, and *j* representing the physical direction with *N* cells.

2.1. Comminution

The first rule describes comminution (the process of grain crushing), which is the predominant factor affecting grainsizes during isotropic compression of brittle granular media [*Einav*, 2007] (Figures 3a and 3d). The comminution rule is set to capture two essential, counteracting mechanisms, correspondingly known as the size [*Weibull*, 1951] and cushioning [*Ben-Nun et al.*, 2010; *Tsoungui et al.*, 1999] effects. They are (1) that smaller grains should be more resilient since they have fewer internal defects (i.e., grains with small $s_{i,j}$ tend to survive) and (2) that grains surrounded by neighbors of similar size are more vulnerable as they tend to carry more internal shear (i.e., grains with small "local polydisperity" $|s_{i,j} - \bar{s}_{i,j}|$ are more likely to crush).

Our rule of comminution is then:

$$\text{if } |s_{i,j} - \bar{s}_{i,j}| \le \beta s_{i,j} : \qquad s_{i,j}(t + \Delta t) = X s_{i,j}(t) \tag{1}$$

where $\bar{s}_{i,j} = (s_{i-1,j} + s_{i+1,j})/2$ is the local average size and β is a nondimensional coefficient controlling the "local fragility" $\beta s_{i,j}$. If the inequality condition is met at time t then the grainsize $s_{i,j}$ reduces over a time increment Δt by the factor X with a rate of breakage r_B, where X is an independent and identically distributed (i.i.d.) random variable drawn uniformly from real numbers in the interval $(0, 1)$. We set Δt such that its product with any rate will be less than unity (here this is applied for r_B, but similarly for other rates, or the most stringent combination thereof).

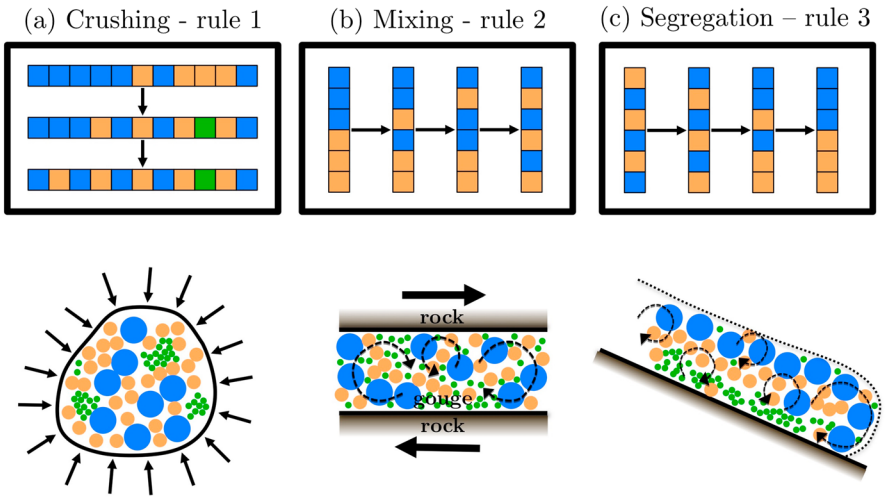

Figure 3. Systems with evolving grainsize distributions. (a–c) The lattice model mechanisms. (d–f) The physical processes described here.

To test the *confined comminution problem* (see Figure 3d), at time $t = 0$ we allocate each cell a size $s_{i,j}$ along $M = 10^6$ cells, but with just one cell in the j direction ($N = 1$), and test how the grainsize distribution evolves over time. We run the simulations until we find a steady state grainsize distribution, which occurs when most of the local polydisperity factors become bigger than the local fragility. Results in Figure 2a show the final grainsize distribution for different β (the only model parameter), plotted in terms of the number of particles $N(\Delta > s)$ with grainsize Δ larger than a certain size s over a log-log curve, which shows a linear trend. Therefore, the slope of this graph is the power law coefficient α of the grainsize distribution: $N(\Delta \geq s) \propto s^{-\alpha}$. We found that α is practically insensitive to the size of the interrogation window throughout which the distribution is measured (up to 10^2 times fewer cells than the overall lattice size). The system is insensitive to the number cells, M, but as with most numerical methods gives smoother results with higher resolution. Therefore, α represents the fractal dimension, which over a wide range of β is around $\alpha = 2$. The inset of Figure 2a shows how the cumulative grainsize distribution by mass, $F = F(s)$, evolves toward an ultimate distribution $F = s^{3-\alpha}$. Power law grainsize distributions with a fractal origin are often evident in earthquake fault gouges (see Figure 1a) [*Marone and Scholz*, 1989; *An and Sammis*, 1994; *Chester et al.*, 2005; *Steacy and Sammis*, 1991; *Billi*, 2005, 2007], and their role as an attractor has been highlighted [*Ben-Nun et al.*, 2010; *Einav*, 2007]. Nevertheless, here the fractal dimension of $\alpha = 2$ is lower than that found in previous investigations where $2.2 < \alpha < 3.2$, but is much closer to comminution observed at lower strain in lab experiments [*Coop et al.*, 2004]. It will be shown later that larger values of α can be produced by combining comminution with mixing.

2.2. Mixing

The second rule describes mixing, which is inevitable in densely sheared granular media where small and large grains often swap places (Figure 3b). This is evidenced by large velocity fluctuations that form vortex-like structures [*Radjai and Roux*, 2002; *Rognon and Einav*, 2010; *Miller et al.*, 2013]. To account for these chaos-like motions, the mixing is activated only along the physical coordinate direction; the internal coordinate is here introduced solely to provide sufficient realizations for a smooth grainsize distribution at any point in space. Here granular mixing takes a symmetric random walk motion in 1-D, where the probabilities of moving to immediate neighbors are the same and develops irrespective of grainsize.

Our rule of mixing is then:

$$s_{i,j} \Leftrightarrow s_{i,j+Y} \tag{2}$$

where Y is a discrete i.i.d. random variable drawn from the two integer values $\{-1, 1\}$ and $\Leftrightarrow$ represents the swapping of values in respective cells. The mixing rate is set to allow random swapping of grains either up or down with diffusion rate $r_D = D/(2\Delta W^2)$, where ΔW^2 is the mean square displacements over which the motion fluctuates [*Campbell*, 1997; *Griffani et al.*, 2013] and D is the granular diffusivity (m^2/s). This is known to scale as $D \propto |\dot{\gamma}|$ for both collisional [*Savage and Dai*, 1993] and dense [*Utter and Behringer*, 2004] flows, where $\dot{\gamma}$ is the local shear strain rate (s^{-1}). Here this rate and therefore D are set to be uniform across the shear layer for simplicity. Figure 4b shows spatiotemporal contours of the local average grainsize of an initially segregated lattice system that mixes over time; the contours have an error of $\pm 1\%$ of the analytical solution of the conventional Fick's diffusion equation shown by superposed lines as

$$\frac{\partial \phi}{\partial t} = \frac{\partial}{\partial z}\left(D\frac{\partial \phi}{\partial z}\right). \tag{3}$$

where $\phi(z, s, t)$ is a probability density function of the grainsizes s, at time t, in a particular physical location z. In other words, using the lattice model with the mixing rule only may be seen as an (inefficient) method to numerically solve the diffusion equation above. However, the advantage of this model is that it can be combined easily with the first and third rules.

2.3. Segregation

The third rule describes segregation (Figure 3c). Unlike fault gouges, granular avalanches occur at low confining pressure and are free to expand while flowing. They can therefore experience large gravity-driven grainsize segregation [*Savage and Lun*, 1988; *Gray and Thornton*, 2005; *Rognon et al.*, 2007; *McElwaine and Nishimura*, 2000; *Naylor*, 1980; *Marks et al.*, 2012]. Many cellular automata have been proposed to describe segregation in granular systems [*Makse et al.*, 1997; *Marks and Einav*, 2011]; however, most use the discrete nature of the cellular automaton to describe the geometry of individual particles and are difficult to homogenize at large scales. We circumvent this issue by using the regular 2-D lattice system described previously.

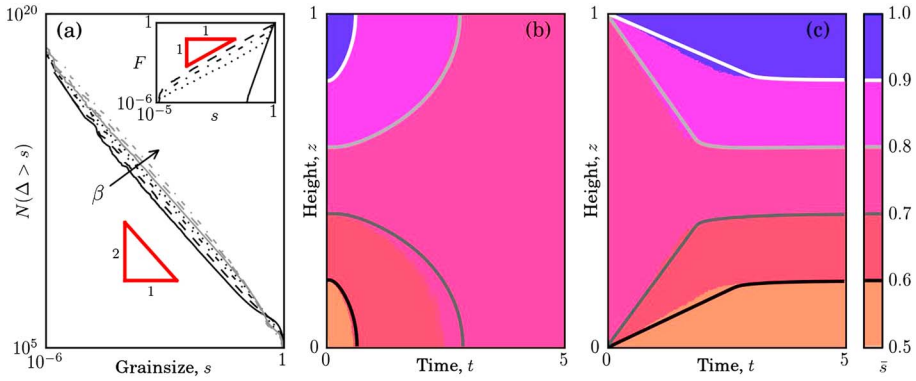

Figure 4. Results from the three lattice model rules tested in isolation. (a) Steady state grainsize distributions using the comminution rule. All simulations begin with a randomly generated initial grainsize distribution with power law dimension $\alpha = -2$ and have $M = 10^6$ by $N = 1$ cells and $r_B = 1$. β is varied as $\beta = 0.05, 0.1, 0.2, 0.3, 0.4, 0.5$, and 0.6. Inset indicates evolution of the grainsize distribution for $\beta = 0.2$ for $t = 0, 0.05, 1, 2$, and 5 (solid, dotted, dash-dotted, and dashed lines, respectively). (b) Average grainsize contours using the mixing rule where $D = 0.05$. The system is initially fully segregated and is composed of a uniform distribution of particles by size between $s = 0.5$ and 1. Superposed lines indicate numerical solution of the corresponding diffusion equation by a finite difference scheme. (c) Average grainsize contours using the segregation rule where $k_S = 1$. The system is initially mixed, with the same distribution of particles as the final state of Figure 4b. Superposed lines indicate numerical solution of the corresponding advection equation presented in [*Marks et al.*, 2012] by the numerical method described therein.

Our new segregation rule for polydisperse media generalizes a previous model for bidisperse media [*Marks and Einav*, 2011], which successfully reproduced the continuum mechanics results in [*Gray and Thornton*, 2005]. Unlike the mixing rule, here the swapping of grains is made preferentially: particles smaller or larger than both their local average ($\bar{s}_j$ averaged along the whole i coordinate) and their swapping partner go down or up, respectively.

Our rule of segregation is then:

$$\begin{aligned} &\text{if } (s_{i,j} < \bar{s}_j) \wedge (s_{i,j} < s_{i,j-1}) : s_{i,j} \Leftrightarrow s_{i,j-1} \\ &\text{if } (s_{i,j} > \bar{s}_j) \wedge (s_{i,j} > s_{i,j+1}) : s_{i,j} \Leftrightarrow s_{i,j+1} \end{aligned} \tag{4}$$

where the statement $A \wedge B$ is true if A and B are both true; else it is false. Motivated by our previous continuum mixture theory of segregation in polydisperse granular media [*Marks et al.*, 2012] the segregation rate is set to depend on grainsize as $r_S = k_s|\dot{\gamma}(s_{i,j} - \bar{s}_j)|/(\Delta W \bar{s}_j)$, with k_s being a constant (m) and $\dot{\gamma}$ is set to be uniform across the shear layer for simplicity. We iterate in two half time steps, alternately applying this rule first to odd rows, and then even rows, such that particles can move at most two cells in a single time step. Without the half stepping, a single particle could migrate unphysically far, due to it swapping location multiple times. Figure 2c shows spatiotemporal contours of the local average grainsize of an initially uniform system normal to the flow direction, which segregates over time; the contours resulting from the lattice model have a typical error of ±1% from the direct numerical solution of the advection equation of the equivalent continuum theory shown by superposed lines as

$$\frac{\partial \phi}{\partial t} = k_s \frac{\partial}{\partial z}\left(\frac{\phi|\dot{\gamma}|(s - \bar{s})}{\bar{s}}\right) \tag{5}$$

As we demonstrated for the case of the mixing rule, using the lattice model with the segregation rule only is shown to represent a good numerical solution to the (nontrivial) advection equation above.

Next, we address the *earthquake fault problem*. In Figure 4a we showed a power law grainsize distribution with fractal dimension $\alpha = 2$ using the comminution rule. A similar comminution rule was proposed before for a 3-D cellular automaton by *Steacy and Sammis* [1991], who found $2 < \alpha < 2.8$ that is closer to the measured range from natural (cataclastic) fault gouge materials of $2.2 < \alpha < 3.2$ [*Marone and Scholz*, 1989; *Chester et al.*, 2005; *Billi*, 2005, 2007]. However, in plane shear confined by walls, mixing of grains inevitably develops, and in our view this phenomenon cannot be neglected from the grainsize dynamics (portrayed in Figure 3e), as it continuously changes packing geometries. To address this point we integrate the rules

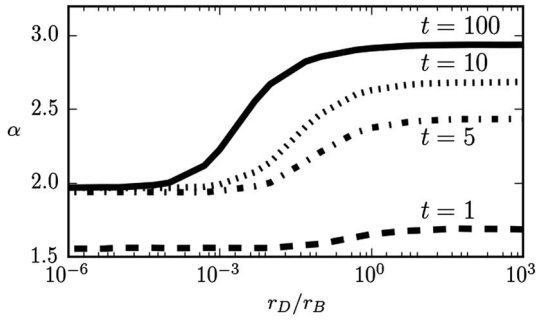

Figure 5. Coupled comminution and mixing rules, applicable for earthquake fault gouges. Varying values of $r_D/r_B = D/(2k_b\Delta W^2)$. For all cases, the system has $M = 1000$ by $N = 101$ cells and $\beta = 0.2$. Plot shows final value of best fit to power law part of cumulative grainsize distribution at $t = 1$, 5, 10 and 100, corresponding to the dashed, dash-dotted, dotted, and solid lines, respectively.

of comminution and mixing to work along the internal and physical shear plane directions of the 2-D lattice, respectively. We set $r_B = k_B|\dot{\gamma}|$ for the fault problem, with k_B being a nondimensional constant, and $\dot{\gamma}$ the shear strain rate across the fault gouge layer. Figure 5 shows how the fractal dimension α can always progress toward 3, at a rate controlled by the dimensionless ratio $R = r_D/r_B$. At $R \ll 1$ (low diffusion rate relative to the breakage rate), the system quickly reaches $\alpha \to 2$, as significant mixing has not yet occurred. Beyond $R > 1$, the fractal dimension becomes insensitive to increasing R but depends on the shear time and approaches $\alpha = 3$. At intermediate Rs, we observe a transition in the fractal dimension from 2 to 3 over time, which may explain observations of $2.2 < \alpha < 3.2$ in natural faults. Compare these predictions with the field measurements shown in Figure 1b, where increasing deformation correlates strongly with increasing values of α. Values of $\alpha > 3$ imply that a minimum particle size is present, below which the power law is no longer a good fit [*Billi*, 2007]. For simplicity, we have not included such a criteria in our model. In earthquake faults, the most comminuted particles lie closer to the fault surface [*Billi*, 2010]; this shows variation of grainsize in space but is due to shear localization and not the preferential sorting of grains.

Unlike in earthquake faults, segregation in the *avalanche problem* cannot be ignored as there is preferential sorting of grains between shear layers (Figure 3f). For this purpose we integrate all three model rules into the lattice system simultaneously. Figure 6 shows the spatiotemporal contours of the local average grainsize and steady state grainsize distributions at three different depths along the shear plane. For large ratios of the segregation and breakage rates (large k_S/k_B) we generally find depth-dependent lognormal distributions, even in the absence of mixing (when the comminution is accompanied by segregation only). Evidence of bimodality is seen at the shallower layers, which vanishes at deeper layers, where the distribution is purely lognormal. These results make qualitative agreement with the grainsize distributions presented in Figures 1c–1f. Quantitative agreement, however, is hard to achieve, as we expect the lognormal distributions to vary in both position and time.

By adopting different combinations of three lattice model rules (crushing, mixing, and segregation) we have been able to reveal a variety of grainsize distributions. The exact form of each distribution was clearly shown to depend on the rates of crushing, mixing and segregation. We described how despite experiencing huge shear deformations, comminution, and mixing, the grainsize distributions of gravity currents may tend to lognormal distributions due to the presence of segregation. This is contrasted with earthquake faults, where a lack of significant segregation causes the grainsize distribution to evolve toward a fractal scaling.

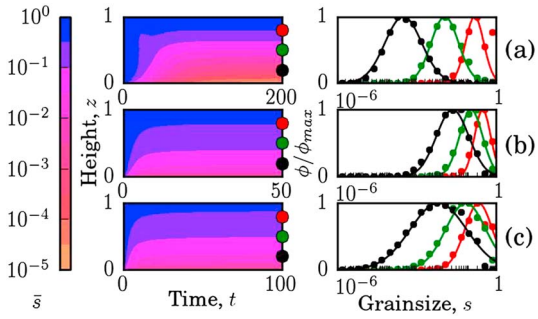

Figure 6. Coupled comminution, mixing and segregation rules, applicable for avalanches and flows. For all cases $r_B = 1$, initial grainsize distribution has $\alpha = -2$ and $\beta = 0.2$. The system has $M = 10000$ by $N = 51$ cells. (a) $k_S = 0.01$, $r_D = 0$. (b) $k_S = 1$, $r_D = 0$, and (c) $k_S = 1$, $r_D = 10$. (left) Average grainsize contours in space and time. (right) Steady state grainsize distributions with superposed lognormal fits; corresponding to three different depths, denoted by circles on the left contours.

3. Discussion

We have expressed segregation and mixing by laws described at the scale of statistically representative volume elements. Therefore, segregation and mixing can be described using continuum models. On the other hand, the comminution model could not simply be coarse grained (or upscaled/homogenized) into a continuum model, since it is governed by finer-scale mechanisms that

depend on the relative positions of individual grains, below the resolution of the representative volume elements. As such, our model provides new means to couple and study the interplay between distinguishable scales: here the representative volume element and the local grain scales. This model can be used to explore the same mechanisms in multiple spatial dimensions if a general velocity field is known.

The field data presented in Figure 1 has been shown to qualitatively match the predictions of the stochastic lattice model presented here. In fault gouges, a connection has been established between the evolution of the gouge material (as it is crushed and mixed) and the value of the fractal dimension of the grainsize distribution. For gravity currents such as snow avalanches, pyroclastic flows, debris flows, and rock avalanches, segregation has been shown to facilitate the production of lognormal grainsize distributions, coupled together with comminution (with or without mixing).

There may well be other factors contributing to the emergence of such lognormal grainsize distributions, but they would not exclude the current mechanism. For example, in wet snow avalanches, granules tend to be larger than in dry snow avalanches due to agglomeration via cohesion, but in both cases the grainsize distributions follow a lognormal shape [*Bartelt and McArdell*, 2009]. Other factors include grainsize reduction due to erosion and the effect of the nonuniformity of the velocity distribution along cross sections of the flow. This might have a critical effect on the formation of frontal segregated levee deposits [*Johnson et al.*, 2012] and during heap flows [*Fan et al.*, 2014] but will not change the qualitative nature of our conclusions.

Acknowledgments

We wish to thank Thierry Faug for stimulating discussions on snow avalanches. Financial support for this research from the Australian Research Council through grant DP1096958 is gratefully appreciated. The code used to generate these results is freely available at http://www.benjymarks.com/FlowSLM.

The Editor thanks Andrea Billi and an anonymous reviewer for their assistance in evaluating this paper.

References

An, L.-J., and C. G. Sammis (1994), Particle size distribution of cataclastic fault materials from Southern California: A 3-d study, *Pure Appl. Geophys.*, *143*(1–3), 203–227.

Bagnold, R. A. (1954), Experiments on a gravity-free dispersion of large solid spheres in a Newtonian fluid under shear, *Proc. R. Soc. A*, *225*(1160), 49–63.

Bartelt, P., and B. W. McArdell (2009), Granulometric investigations of snow avalanches, *J. Glaciol.*, *55*(193), 829–833.

Ben-Nun, O., I. Einav, and A. Tordesillas (2010), Force attractor in confined comminution of granular materials, *Phys. Rev. Lett.*, *104*(10), 108001.

Billi, A. (2005), Grain size distribution and thickness of breccia and gouge zones from thin (< 1 m) strike-slip fault cores in limestone, *J. Struct. Geol.*, *27*(10), 1823–1837.

Billi, A. (2007), On the extent of size range and power law scaling for particles of natural carbonate fault cores, *J. Struct. Geol.*, *29*(9), 1512–1521.

Billi, A. (2010), Microtectonics of low-p low-t carbonate fault rocks, *J. Struct. Geol.*, *32*(9), 1392–1402.

Campbell, C. S. (1997), Self-diffusion in granular shear flows, *J. Fluid Mech.*, *348*(1), 85–101.

Chester, J. S., F. M. Chester, and A. K. Kronenberg (2005), Fracture surface energy of the punchbowl fault, San Andreas system, *Nature*, *437*(7055), 133–136.

Coop, M., K. Sorensen, T. B. Freitas, and G. Georgoutsos (2004), Particle breakage during shearing of a carbonate sand, *Géotechnique*, *54*(3), 157–163.

Dunning, S. (2006), The grain size distribution of rock-avalanche deposits in valley-confined settings, *Ital. J. Eng. Geol. Environ.*, *1*, 117–121.

Einav, I. (2007), Fracture propagation in brittle granular matter, *Proc. R. Soc. A*, *463*(2087), 3021–3035.

Esposito, L., A. W. Esposito, A. Pasculli, and N. Sciarra (2013), Particular features of the physical and mechanical characteristics of certain phlegraean pyroclastic soils, *Catena*, *104*, 186–194.

Fan, Y., C. P. Schlick, P. B. Umbanhowar, J. M. Ottino, and R. M. Lueptow (2014), Modelling size segregation of granular materials: The roles of segregation, advection and diffusion, *J. Fluid Mech.*, *741*, 252–279.

Gray, J., and A. Thornton (2005), A theory for particle size segregation in shallow granular free-surface flows, *Proc. R. Soc. A*, *461*(2057), 1447–1473.

Griffani, D., P. Rognon, B. Metzger, and I. Einav (2013), How rotational vortices enhance transfers, *Phys. Fluids*, *25*(9), 093301.

Johnson, C. G., B. P. Kokelaar, R. M. Iverson, M. Logan, R. G. LaHusen, and J. M. N. T. Gray (2012), Grain-size segregation and levee formation in geophysical mass flows, *J. Geophys. Res.*, *117*, F01032, doi:10.1029/2011JF002185.

Makse, H. A., S. Havlin, P. R. King, and H. E. Stanley (1997), Spontaneous stratification in granular mixtures, *Nature*, *386*, 379–382.

Marks, B., and I. Einav (2011), A cellular automaton for segregation during granular avalanches, *Granular Matter*, *13*(3), 211–214.

Marks, B., P. Rognon, and I. Einav (2012), Grainsize dynamics of polydisperse granular segregation down inclined planes, *J. Fluid Mech.*, *690*, 499–511.

Marone, C., and C. Scholz (1989), Particle-size distribution and microstructures within simulated fault gouge, *J. Struct. Geol.*, *11*(7), 799–814.

McElwaine, J., and K. Nishimura (2000), Size segregations in snow avalanches, in *IUTAM Symposium on Segregation in Granular Flows*, pp. 81–88, Springer, Netherlands.

Miller, T., P. Rognon, B. Metzger, and I. Einav (2013), Eddy viscosity in dense granular flows, *Phys. Rev. Lett.*, *111*(5), 058002.

Naylor, M. A. (1980), The origin of inverse grading in muddy debris flow deposits—A review, *J. Sediment. Res.*, *50*(4), 1111–1116.

Phillips, C. J., and T. R. Davies (1991), Determining rheological parameters of debris flow material, *Geomorphology*, *4*(2), 101–110.

Pollet, N., and J.-L. Schneider (2004), Dynamic disintegration processes accompanying transport of the Holocene Flims sturzstrom (Swiss Alps), *Earth Planet. Sci. Lett.*, *221*(1), 433–448.

Radjai, F., and S. Roux (2002), Turbulent-like fluctuations in quasistatic flow of granular media, *Phys. Rev. Lett.*, *89*(6), 064302.

Rognon, P., and I. Einav (2010), Thermal transients and convective particle motion in dense granular materials, *Phys. Rev. Lett.*, *105*(21), 218–301.

Rognon, P. G., J.-N. Roux, M. Naaïm, and F. Chevoir (2007), Dense flows of bidisperse assemblies of disks down an inclined plane, *Phys. Fluids*, *19*, 058101.

Savage, S., and R. Dai (1993), Studies of granular shear flows. wall slip velocities, 'layering' and self-diffusion, *Mech. Mater.*, *16*(1), 225–238.
Savage, S., and C. Lun (1988), Particle size segregation in inclined chute flow of dry cohesionless granular solids, *J. Fluid Mech.*, *189*, 311–335.
Schmincke, H.-U. (1967), Graded lahars in the type sections of the Ellensburg Formation, south-central Washington, *J. Sediment. Res.*, *37*(2), 438–448.
Steacy, S. J., and C. G. Sammis (1991), An automaton for fractal patterns of fragmentation, *Nature*, *353*(6341), 250–252.
Tsoungui, O., D. Vallet, and J.-C. Charmet (1999), Numerical model of crushing of grains inside two-dimensional granular materials, *Powder Technol.*, *105*(1), 190–198.
Utter, B., and R. P. Behringer (2004), Self-diffusion in dense granular shear flows, *Phys. Rev. E*, *69*(3), 031308.
Weibull, W. (1951), A statistical distribution function of wide applicability, *J. Appl. Mech.*, *18*(3), 293–297.
Wilson, C. (1985), The taupo eruption, New Zealand II. The taupo ignimbrite, *Proc. R. Soc. A*, *314*, 229–310.